applied sciences

MDPI

Article

Evaluation on Improvement Zone of Foundation after Dynamic Compaction

Chong Zhou [1], Chenjun Yang [1], Hui Qi [1,2], Kai Yao [1,*], Zhanyong Yao [1,*], Kai Wang [2], Ping Ji [2] and Hui Li [1]

[1] School of Qilu Transportation, Shandong University, Jinan 250061, China; zhouchong@mail.sdu.edu.cn (C.Z.); yangchenjun@mail.sdu.edu.cn (C.Y.); 1016913282@qq.com (H.Q.); huili_sdu@163.com (H.L.)

[2] Shandong HI-SPEED Group, Jinan 250014, China; sdgswangkai@163.com (K.W.); 921055979@qq.com (P.J.)

* Correspondence: yaokai@sdu.edu.cn (K.Y.); zhanyong-y@sdu.edu.cn (Z.Y.)

Abstract: Dynamic compaction (DC) is one of the most popular methods for ground improvement. To solve the problem of the factors affecting the sandy soil improvement effect and estimate the effective improvement range under DC, the influences of drop number, drop energy, tamping distance, tamper radius, and drop momentum on the relative degree of improvement were investigated. Three normalized indicators $\Delta\delta_{z,i}$, $\Delta\delta_{A,i}$, and $\Delta\delta_{U,i}$ were derived to evaluate the weak zone and corresponding improvement effect. For multipoint tamping, it is found that the improvement depth and the improvement of the weak zone are highly correlated with drop energy and drop momentum, while the influence of the drop number and tamper radius is relatively smaller. The improvement of the weak zone and the improvement depth decrease with tamping distance, whereas the improvement area increases with tamping distance. The soil compacted by the previous impact point will be improved to a lesser extent with impact at subsequent impact points. It is also noted that drop energy had better not exceed the saturated drop energy in DC design. Based on the parametric study, a formula considering the various factors of DC was put forward, with the validation by two field cases of DC.

Keywords: dynamic compaction; design parameters; improvement depth; multipoint tamping; prediction formula

Citation: Zhou, C.; Yang, C.; Qi, H.; Yao, K.; Yao, Z.; Wang, K.; Ji, P.; Li, H. Evaluation on Improvement Zone of Foundation Improved by Dynamic Compaction. *Appl. Sci.* **2021**, *11*, 2156. https://doi.org/10.3390/app11052156

Academic Editors: Stefano Dal Pont and Matthieu Briffaut

Received: 30 December 2020
Accepted: 23 February 2021
Published: 28 February 2021

1. Introduction

Dynamic compaction (DC) is a commonly used method to improve the bearing capacity of various kinds of soils [1–5]. At present, the most commonly used design approach is Menard's [6] framework, which is entirely empirical with low accuracy for predicting the improvement depth. Moreover, site-dependent parameters such as soil properties as well as equipment factors [7,8] like tamping distance, tamper radius, tamper shape, and drop number may also influence the improvement depth of the compacted soil. Up to now, a significant amount of numerical studies [9–12], physical model tests [13,14], and field tests [1,15–18] have been reported on the improvement depth of DC; however, the majority of these works mainly focused on the improvement range below the tamper and only dealt with the soil response by single-point tamping. In reality, the layout of DC improvement is typically in a rectangular or triangular grid pattern to conduct multipoint tamping. In terms of multipoint tamping, Chow et al. [19] proposed an empirical method for assessing the compaction effect between impact points, which is based on the relationship between normalized friction angle and dimensionless distance by single-point tamping. Two design approaches to choose the tamping distance of DC were presented. However, the assumption of a constant frictional angle along with depth may lead to an inaccurate prediction of the tamping distance. Jahangiri [20] proposed a novel method to determine the corresponding tamping distance. Although the forecasting

methods have made great progress, compared with the method of Chow et al. [19], the assumption of asymmetry in a compacted zone around the centerline of the impact point causes limitations on the feasibility of tamping distance. Wang et al. [21] used the LS-DYNA software to study multipoint tamping in granular soils. However, they only modeled two blows at each impact point, which is far from enough to ensure the stabilization of the DC. Dou [22] also proposed a method to estimate the relative density with the depth between impact points. However, the assessment curve must be benchmarked by five special points and the relevant crater depth has to be estimated first. Several sandy field tests have shown that the triangular grid patterns are more efficient than the rectangular grid patterns in the case of small areas of DC treatment [23–26]. However, those field investigations aim to come up with the DC construction parameters based on some specific project cases, which may be not suitable for other projects. In general, a reasonably comprehensive design framework that can account for different sandy soil properties and construction parameters to guide the practical DC design for multipoint tamping remain unavailable.

In this paper, a three-dimensional finite element analysis with an improved cap soil model was conducted to simulate the single-point and the multipoint tamping on dry sandy ground. The numerical analysis was first validated by using centrifuge model results from the published literature, then the influences of drop energy, drop number, tamper radius, tamping distance, as well as drop momentum on the relative degree of improvement, were discussed in detail. After that, a prediction formula considering the factors affecting relative degree of sandy soil improvement was proposed based on the simulation results. Finally, the accuracy and reliability of the proposed formula were validated by using the sandy field test results. It should be noted that the soils studied in this paper are moist and dry granular soils with high permeability, which can be assumed to be dry soil; saturated or unsaturated soils are not involved.

2. Numerical Model for DC

2.1. Soil Constitutive Model

The soil constitutive relation adopted in this study is the cap yield hardening model, which has a shearing surface and a hardening cap with good feasibility of analyzing the DC [9–12]. As Figure 1 shows, a Drucker–Prager shearing surface used herein is given by

$$F_s = q - p' \tan \beta - d = 0 \tag{1}$$

where p' and q are the mean effective and deviator stresses in p'–q plane, respectively. Parameters d and β in the p'-q plane (shown in Figure 1) are two material constants defined as follows:

$$\tan \beta = \frac{2 \sin \phi'}{\sqrt{3}\left(3 - \sin \phi'\right)}, d = \frac{6c' \cos \phi'}{\sqrt{3}\left(3 - \sin \phi'\right)} \tag{2}$$

where φ' is the angle of friction and c' is the cohesion, which are directly obtained from τ–s' plane.

And an elliptic hardening equation is given by

$$F_c = \sqrt{\left(p' - p_a\right)^2 + \left(R'q\right)^2} - R'\left(d + p_a \tan \beta\right) = 0 \tag{3}$$

where R' is the elliptic eccentricity that controls the shape of the cap surface. The evolution parameter p_a is the point at which the shear surface intersects with the cap surface, which is given by

$$p_a = \frac{p_b - R'd}{1 + R' \tan \beta} \tag{4}$$

where p_b is the intersection point between the cap surface and the p'- axis and is related to the plastic volumetric strain ε_v^p by

$$p_b = \frac{1}{3}\left(-\frac{1}{D'}\ln\left(1-\frac{\varepsilon_v^p}{W'}\right)\right)+p_0 \quad (5)$$

in which D' and W' are the hardening parameters acquired by odometer tests, and p_0 is the initial in situ mean effective stress.

In this study, a subroutine is developed to simulate the variation of soil's modulus with successive blows. The bulk modulus K' is updated based on using the empirical relationship derived by Ghassemi [28] and Poran et al. [29]

$$K' = \eta \exp(\kappa D_r) P_{ap}\left(\frac{p'}{P_{ap}}\right)^{0.5} \quad (6)$$

where P_{ap} is the atmospheric pressure; D_r is the relative density; η and κ are the empirical parameters. Table 1 presents the parameters of the cap model obtained from the previous numerical studies based on the centrifuge tests [9,10]. The initial elastic modulus of the soil E' is 25 MPa, with the Poisson ratio υ' of 0.25.

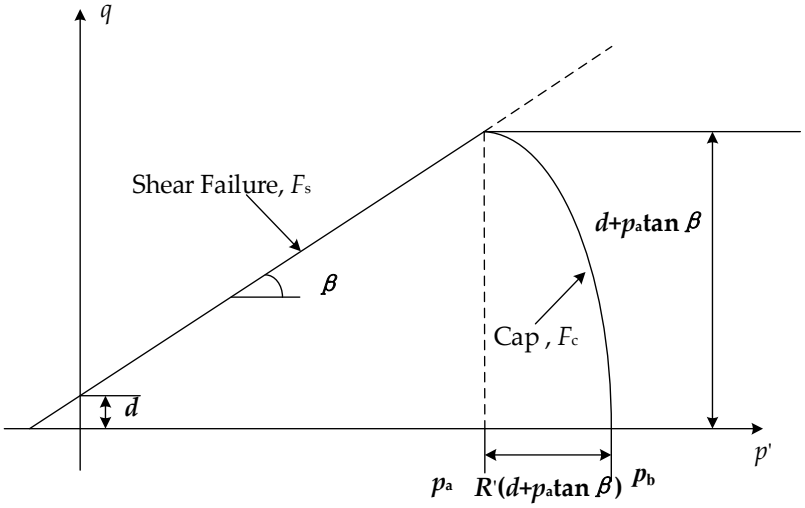

Figure 1. Yield surface of cap model in p'–q plane [27].

Table 1. Parameters of the cap model.

Coordinate System	c' (kPa)	φ'	R	W'	D' (m²/kN)	η	κ
p'-q	0	30.0°	0.83	0.4	1.8×10^{-4}	120	0.0134

2.2. Validation of the Numerical Model

Oshima and Takada [13] conducted a centrifuge model test to investigate soil improvement by DC. The dimension of the cylindric prototype of the sandy ground is 18 m in depth and 28 m in diameter. The tamper with a weight of 20 tons and a diameter of 2.4 m is dropped from a height of 20 m. A three-dimensional (3D) finite element (FE) model is established to simulate the test of Oshima and Takada [13], as shown in Figure 2, where the drop energy is simulated by applying an impact velocity of 20 m/s on the tamper. The Young's modulus and Poisson ratio of the tamper are 90 GPa and 0.3, respectively. The boundary of the cylinder is fixed in the horizontal direction and free in the vertical direction ($U_x = U_y = 0$, see Figures 2 and 5). The bottom boundary is fixed in two horizontal and vertical directions ($U_x = U_y = U_z = 0$, see Figures 2 and 5). The corresponding model for

sandy soil consists of 118680 (C3D8R) 8-node brick elements and 124127 nodes. Furthermore, infinite elements (CIN3D8) in ABAQUS [27] are used to minimize wave reflection from the boundary of FE domains during DC.

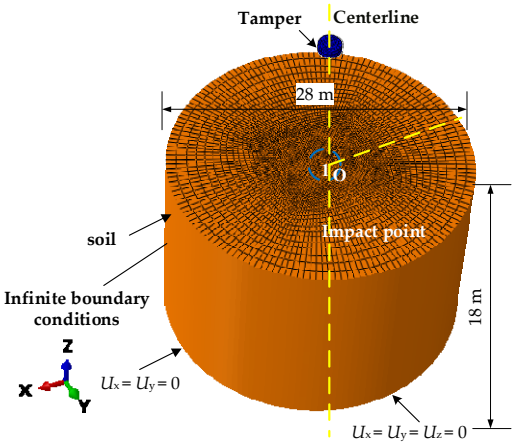

Figure 2. The numerical simulation model and finite element mesh.

As Figure 3 shows, the shapes of the improved zone from the simulation are similar to those from centrifuge model tests. The numerical data indicate a smaller zone of highly compacted soil having an increase in relative density of 40% or greater. This can be attributed to the hardening parameters used in the analyses and the soil undergoes a stiffening process along with the increase in the drop number. Four sets of the hardening parameters (Table 2) were studied to assess the influence of hardening parameters on the zone of compaction.

Table 2. Typical hardening parameters for granular soils.

Case Number	ρ_s(kg/m³)	W'	D' (m²/kN)	Dense Degree
1	1500	0.4	2.2×10^{-4}	Loose
2	1500	0.4	1.8×10^{-4}	Slightly dense
3	1500	0.22	3.0×10^{-5}	Medium dense
4	1500	0.18	1.0×10^{-6}	Dense

Figure 4a shows the improvement depth corresponding to $\Delta D_r = 10\%$ for cases 1 to 3 are 8.23, 5.7, and 3.0 m, indicating that the effective improvement depth decreases with the increase in the hardening parameters and the hardening parameters of case 2 used in the analyses agree well with that measured in centrifuge test. Moreover, the maximum value of ΔD_r for case 4 is only 6%, which has been ignored in Figure 4a. Figure 4b shows the range of soil improvement also decreases with the increase in the hardening parameters under the same condition of $\Delta D_r = 5\%$. Thus, the smaller zone with $\Delta D_r = 40\%$ can be attributed to the hardening parameters used in the analyses. On the other hand, a close agreement of crater depth between the centrifuge test and numerical results is obtained (See Figure 5), indicating that it is reliable to use this improved soil cap model to analyze the DC problems of multipoint tamping.

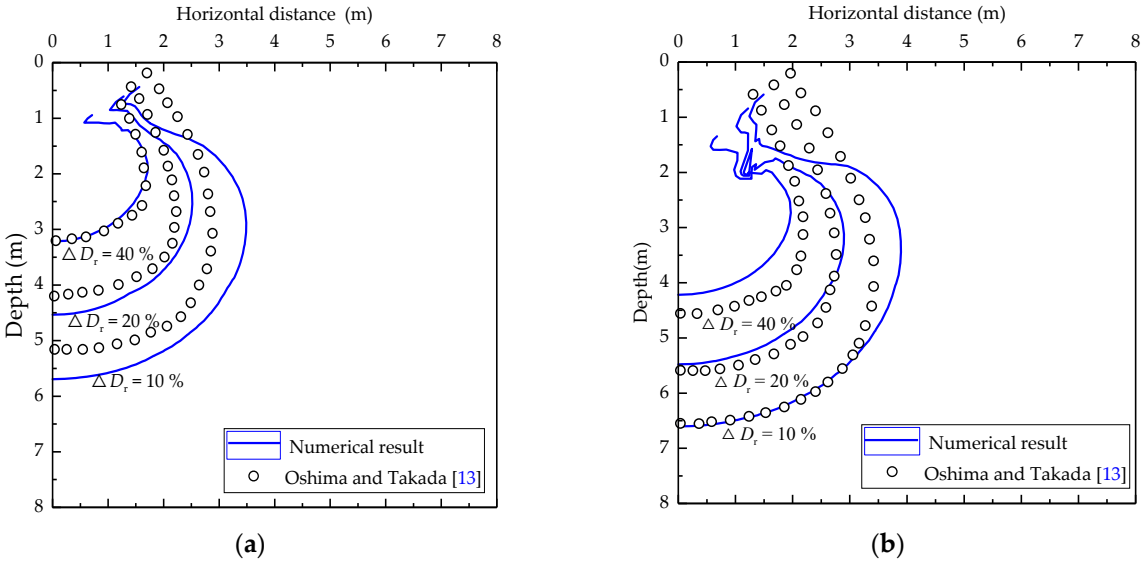

Figure 3. Comparison of increment in relative density: (**a**) after 5 blows; (**b**) after 10 blows.

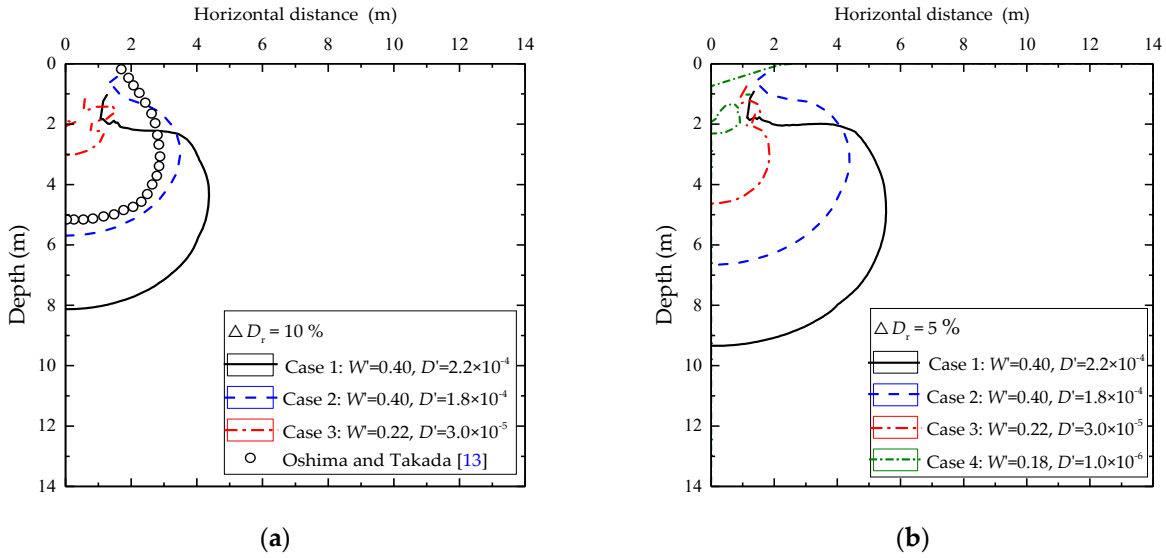

Figure 4. The effect of the hardening parameters on ΔD_r after 10 blows: (**a**) ΔD_r =10%; (**b**) ΔD_r = 5%.

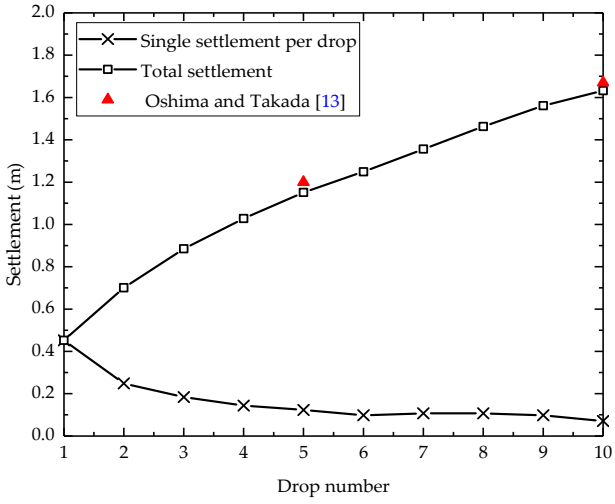

Figure 5. Comparison of settlement.

3. Parametric Studies

A parametric study was performed to analyze the influences of drop number, drop energy, tamper radius, tamping distance, and the different combinations of tamper mass and drop height on the soil's degree of improvement for both single-point and multipoint tamping. The operational parameters in all cases were shown in Table 3. The parameters listed in Table 1 were also used to simulate multipoint tamping.

Table 3. Summary of operational parameters in the simulation.

Case Number	Drop Energy, $M \times H$ (kN·m)	Tamper Mass, M (tons)	Drop Height, H (m)	Drop Number, (N)	Tamper Diameter, D (m)	Tamping Distance, S (m)
1	2000	10	20	10	2.4	6.0 (2.5 D)
2	4000	20	20	10	2.4	6.0 (2.5 D)
3	6000	30	20	10	2.4	6.0 (2.5 D)
4	8000	40	20	10	2.4	6.0 (2.5 D)
5	10000	50	20	10	2.4	6.0 (2.5 D)
6	4000	20	20	10	1.2	6.0 (5.0 D)
7	4000	20	20	10	3.2	6.0 (1.875 D)
8	4000	20	20	10	4.0	6.0 (1.5 D)
9	4000	20	20	10	4.8	6.0 (1.25 D)
10	4000	20	20	10	6.0	6.0 (1.0 D)
11	4000	20	20	10	2.4	3.6 (1.5 D)
12	4000	20	20	10	2.4	8.4 (2.0 D)
13	4000	20	20	10	2.4	10.8 (2.5 D)
14	4000	15	26.6	10	2.4	6.0 (2.5 D)
15	4000	30	13.4	10	2.4	6.0 (2.5 D)
16	4000	40	10	10	2.4	6.0 (2.5 D)
17	4000	50	8	10	2.4	6.0 (2.5 D)

3.1. Description of the Simulation Cases for Multipoint Tamping

As shown in Figure 6, section A-A is the symmetry plane of the two impact points, from which the contour lines are extracted. The number of each of impact points 1 and 2 represents the tamping sequence, which means DC will be conducted on point 2 after point 1. Each impact point is subjected to 10 blows of DC. It should be noted that point 3 locates at the middle of points 1 and 2 is the monitoring point, which is not subjected to any blow.

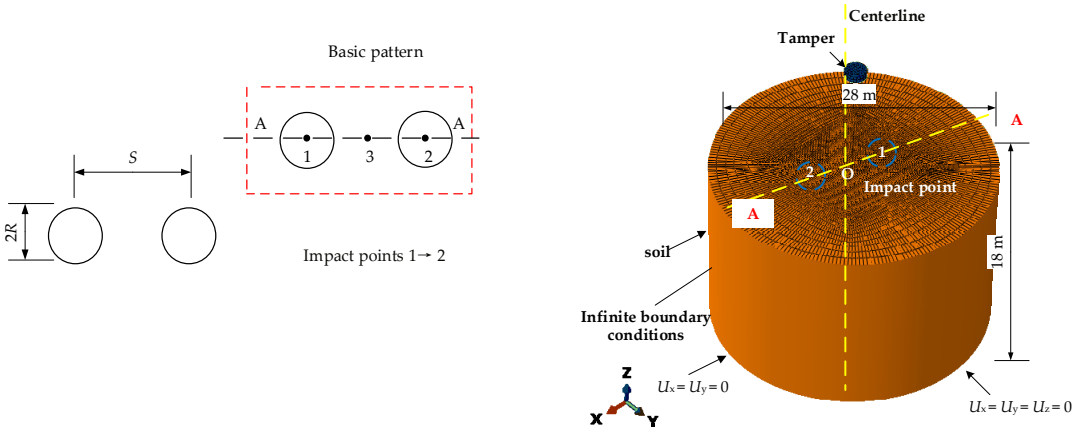

(**a**) (**b**)

Figure 6. The layout of the multipoint tamping and 3D FE mesh: (**a**) the layout; (**b**) 3D FE mesh.

The effect of DC is evaluated by the relative degree of improvement I_r [10]

$$I_r = \frac{D_r - D_{r0}}{100 - D_{r0}} \times 100(\%) \quad (7)$$

where D_r is the relative density, D_{r0} is the initial relative density before DC. The effect of soil properties in this study was not considered as Lee and Gu [10] concluded that the influence of soil types and properties on the compaction effect can be removed by using I_r. Following Gu and Lee [9], Lee and Gu [10], and Oshima and Takada [13], the improvement depth is taken to be the depth where the incremental relative density ΔD_r was 5%. A 5% change in the relative density of sand leads to a change of about 7.7% in the relative degree of improvement I_r, based on Equation (7).

Three normalized indicators $\Delta\delta_{z,i}$, $\Delta\delta_{A,i}$, and $\Delta\delta_{U,i}$ were derived to evaluate the weak zone and the corresponding improvement effect. Table 4 shows the meaning of the normalized indicators and how they are used to evaluate the sandy soil improvement in the following analysis.

Table 4. The meaning of normalized indicators.

Notation	Formula Definition	Physical Meaning
$S'_i(i=1,2)$	$S'_i = \frac{\int_a^b f(I_r, \text{depth})\,d(\text{depth})}{(b-a)} \quad (i=1,2)$ where a = 0 m means the ground surface; b = 18 m means the depth at 18 m from the ground surface.	S'_1 and S'_2 are the mean value theorem of integral computation results between I_r and depth after tamping of the 1st and 2nd impact points.
$Z'_i(i=1,2)$	-	Z'_1 and Z'_2 are the improvement depth corresponding to I_r = 7.7% after tamping of the 1st and 2nd impact points.
$A'_i(i=1,2)$	-	A'_1 and A'_2 are the improvement area corresponding to the zone of I_r = 7.7% after tamping the 1st and 2nd impact points.
S'_R, Z'_R, and A'_R	-	Three standard values based on the case of the numerical model with S = 6.0 m, MH = 4000 kN·m, R = 1.2 m after the completion of the 1st impact points.
$\delta_{U,i}(i=1,2)$	$\delta_{U,i} = \frac{S'_i}{S'_R}(i=1,2)$	$\delta_{U,1}$ and $\delta_{U,2}$ are the normalized mean values of I_r after tamping of the 1st and 2nd impact points.
$\delta_{z,i}(i=1,2)$	$\delta_{z,i} = \frac{Z'_i}{Z'_R}(i=1,2)$	$\delta_{z,1}$ and $\delta_{z,2}$ are the normalized improvement depth after tamping of the 1st and 2nd impact points.
$\delta_{A,i}(i=1,2)$	$\delta_{A,i} = \frac{A_i}{A'_R}(i=1,2)$	$\delta_{A,1}$ and $\delta_{A,2}$ are the normalized improvement area after tamping of the 1st and 2nd impact points.
$\Delta\delta_{U,i}(i=1,2)$	$\Delta\delta_{U,1}=\delta_{U,1}, \Delta\delta_{U,2} = \delta_{U,2} - \delta_{U,1}$	$\Delta\delta_{U,1}$ and $\Delta\delta_{U,2}$ are used to investigate the soil improvement below point 3 (between impact points) during impact at points 1 and 2, respectively.
$\Delta\delta_{z,i}(i=1,2)$	$\Delta\delta_{z,1}=\delta_{z,1}, \Delta\delta_{z,2} = \delta_{z,2} - \delta_{z,1}$	$\Delta\delta_{z,1}$ and $\Delta\delta_{z,2}$ are used to investigate improvement depth during impact at points 1 and 2, respectively.
$\Delta\delta_{A,i}(i=1,2)$	$\Delta\delta_{A,1}=\delta_{A,1}, \Delta\delta_{A,2} = \delta_{A,2} - \delta_{A,1}$	$\Delta\delta_{A,1}$ and $\Delta\delta_{A,2}$ are used to investigate the improvement area corresponding to the zone of I_r = 7.7% during impact at points 1 and 2, respectively.

3.2. Effect of Drop Number

The numerical simulation of DC is performed with tamping distance S = 6.0 m, drop energy MH = 4000 kN·m, tamper radius R = 1.2 m, and blows of 10 at each impact point to investigate the effect of the drop number on the soil improvement.

As shown in Figure 7a, with the increase in drop number, it is observed that there is a gradually increasing trend in the improvement zone of DC. Whereas the incremental values generally decrease until about 8–10 blows, when the drop number becomes essentially insignificant for single-point tamping. This implies that there is a "saturation" stage in DC. The reason is that the soil is relatively loose in the early few blows, which is beneficial for absorbing drop energy. However, as the soil is compacted gradually, the improvement effect begins to be weakened. Figure 7b shows a similar tendency for multipoint tamping. However, the zone below point 1 in the right part has not changed during the impact at point 2, indicating that the impact at point 2 has almost no effect on the I_r beneath point 1 with S = 6.0 m.

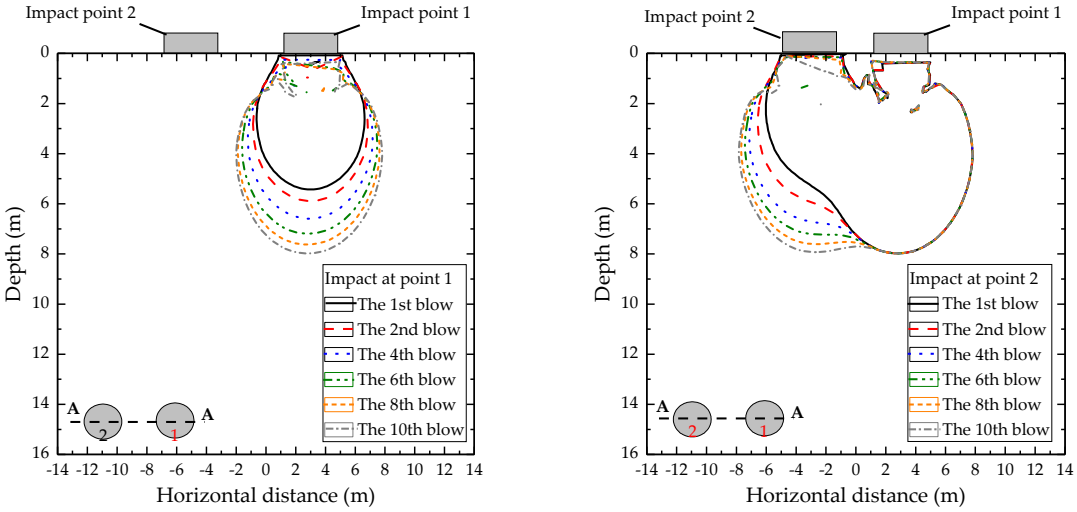

(**a**) (**b**)

Figure 7. The zone of I_r = 7.7% for drop number: (**a**) impact at point 1; (**b**) impact at point 2.

Figure 8a shows that the value of I_r commonly increases as the drop number increases, but the incremental value of I_r generally decreases. The value of I_r at the first six blows increases remarkably, whereas the subsequent blows do not induce an obvious change of I_r, which is consistent with the observations of other researchers [17,18]. Figure 8b shows that the value of I_r below point 3 always increases with the increasing drop number. However, the final value of I_r below point 3 (especially for the upper layer) is still lower than that of point 1, indicating that a relatively weak zone exists between impact points. This finding is consistent with the results of Chow et al. [19], Wang et al. [21], and Dou [22]. Moreover, the value of I_r along the depth decays rapidly for single-point tamping, while for multipoint tamping, the value of I_r increases along with the depth within around 3 m where the maximum value of I_r occurs. Beyond the depth of 3 m, I_r decreases with depth. This may be due to the effect of the stress wave (surface wave) at the bottom of the tamper diffusing along a certain angle and lateral confinement effect, resulting in a weak zone in the upper soil layer [30], where it requires a further impact at the intermediate point between the impact points of the first pass in DC.

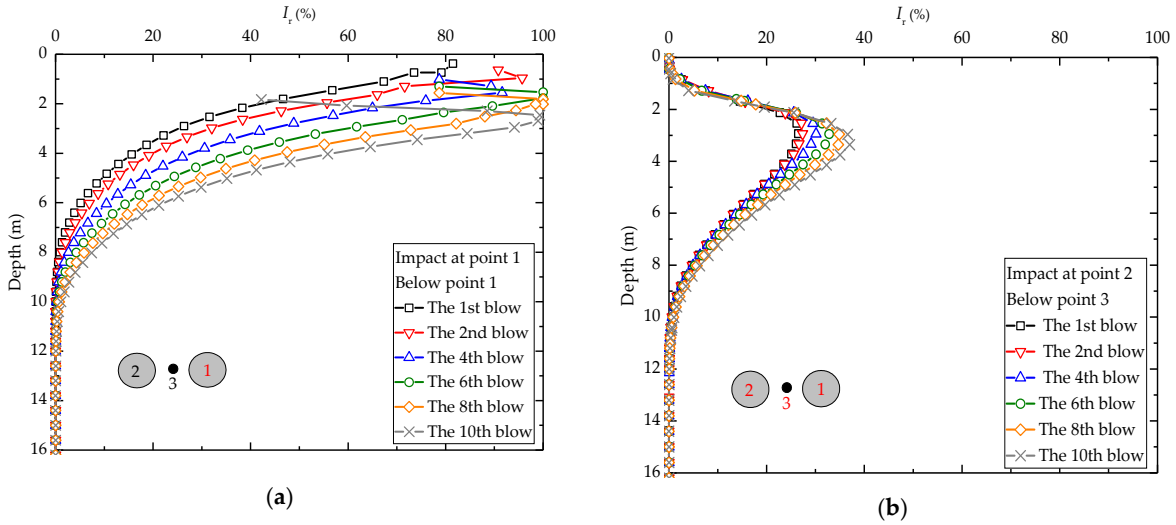

Figure 8. I_r of soil versus depth for drop number: (**a**) below impact point 1; (**b**) below impact point 3.

Figure 9 shows that both $\Delta\delta_{z,1}$ and $\Delta\delta_{U,1}$ generally increase with the drop numbers, indicating that the soil improvement between impact points can be improved as DC continues. However, the increasing trend gradually slows down after the eighth blow, which is consistent with the results of Figures 7 and 8. Moreover, for single-point tamping, the first six blows can account for 80% of the improvement effect. It is also noted that $\Delta\delta_{U,1}$ increases from 38% to 100% during impact at point 1, while $\Delta\delta_{U,2}$ only increases from 1% to 10% during impact at point 2. This means that soil improvement between impact points mainly occurs during impact at point 1. The second impact point contributes little to further densification.

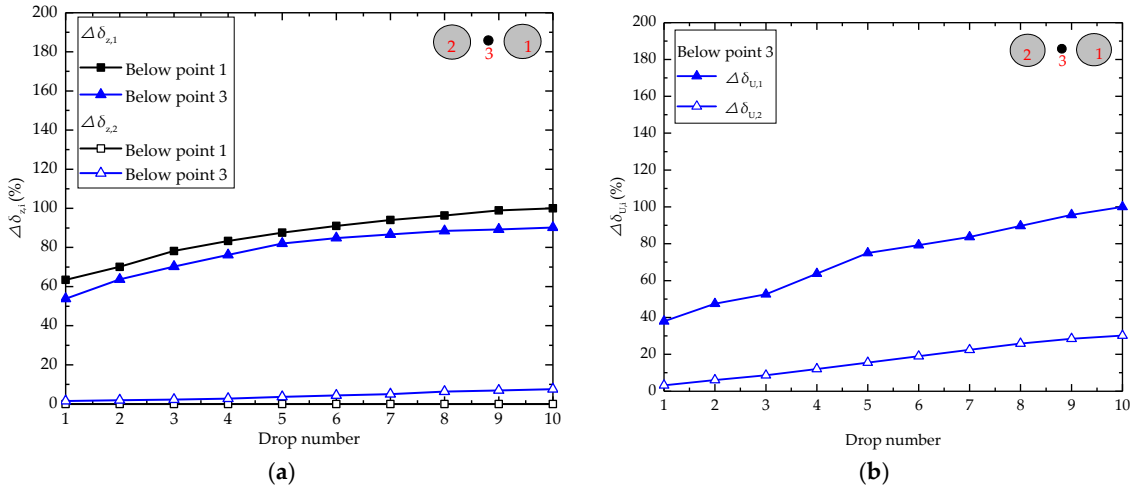

Figure 9. Normalized indicators versus drop number: (**a**) $\Delta\delta_{z,i}$; (**b**) $\Delta\delta_{U,i}$.

3.3. Effect of Drop Energy

The numerical simulation of DC is performed with tamping distance S = 6.0 m, drop energy MH ranging from 2000 to 10000 kN·m, tamper radius R = 1.2 m, and the blows of 10 at each impact point to investigate the effect of the drop energy on the soil improvement.

The zone of I_r = 7.7% for different drop energy is shown in Figure 10. It can be found that with the increase in drop energy, the zone of soil improvement by DC gradually increases. This is consistent with the relative degree of soil improvement shown in Figure 11a. The increased rate of I_r became slow and finally, the value of I_r reaches a stable state

when the drop energy is increased to 8000 kN·m. It is therefore concluded that there exists a "saturation" drop energy beyond which applying further energy has little effect on soil improvement (see Figure 11a). Similar results are also reported by Jia [31]. Figure 11b shows that the increase in drop energy for multipoint tamping can produce a wide range of soil improvement between impact points. This is mainly because sufficient I_r below the tamper has been achieved by single-point tamping. Subsequent impact at point 2 will result in the overlap of the contour line (two reinforced bulbs with a relative degree of improvement I_r, induced by the first and the second impact points overlapping with each other), which is mainly affected by the drop energy (See Figure 22). That is, a higher drop energy leads to a wider range of the overlap of the contour line between the weak zone.

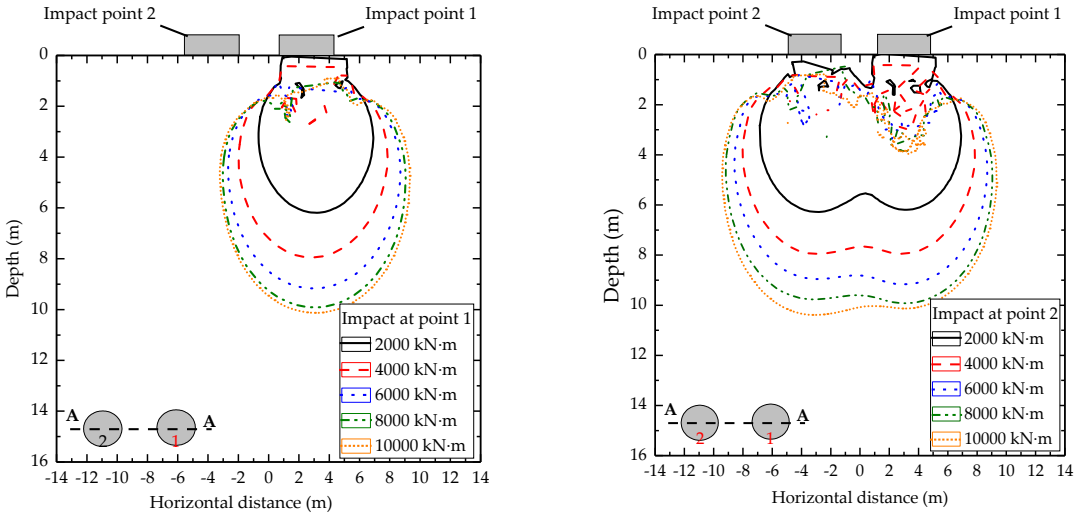

Figure 10. The zone of I_r = 7.7% for drop energy: (**a**) impact at point 1; (**b**) impact at point 2.

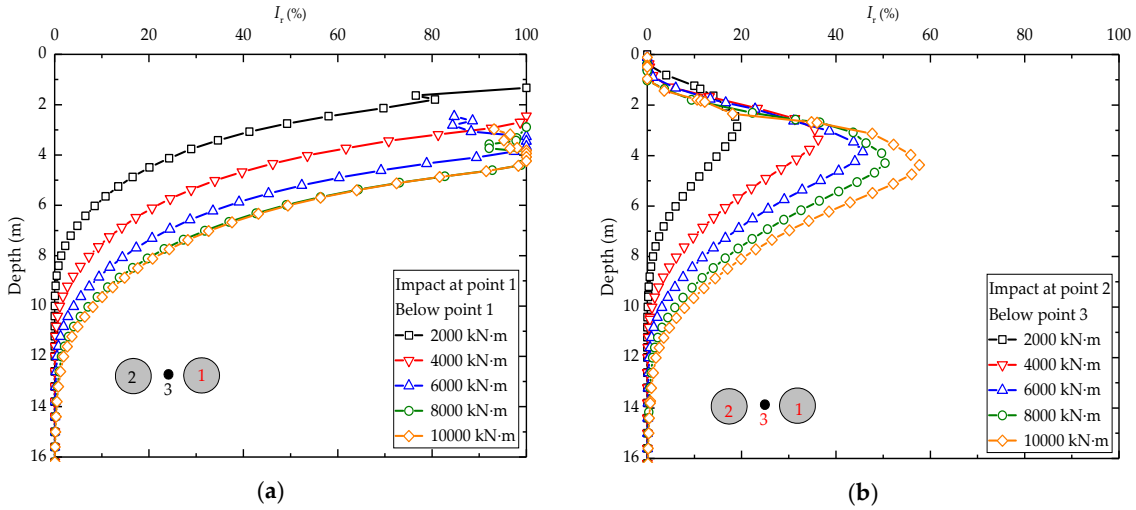

Figure 11. I_r of soil versus depth for drop energy: (**a**) below impact point 1; (**b**) below point 3.

Figure 12 shows that with the increase in drop energy, both $\Delta\delta_{z,1}$ and $\Delta\delta_{U,i}$ (i=1,2) increase continuously, and a marginal increase is observed beyond 8000 kN·m. This indicates that the higher drop energy, the deeper improvement depth, and the better soil improvement between impact points that will be achieved. Again this proves that a further increase in drop energy has little effect on soil improvement. Besides, $\Delta\delta_{U,1}$ increases from 42% when *MH* = 2000 kN·m to 180% when *MH* = 10,000 kN·m during impact at point 1, while $\Delta\delta_{U,2}$ only increases from 24% when *MH* = 2000 kN·m to 50% when *MH* = 10000

kN·m during impact at point 2. This means the first impact points make a greater contribution to the soil improvement between impact points than the second impact point.

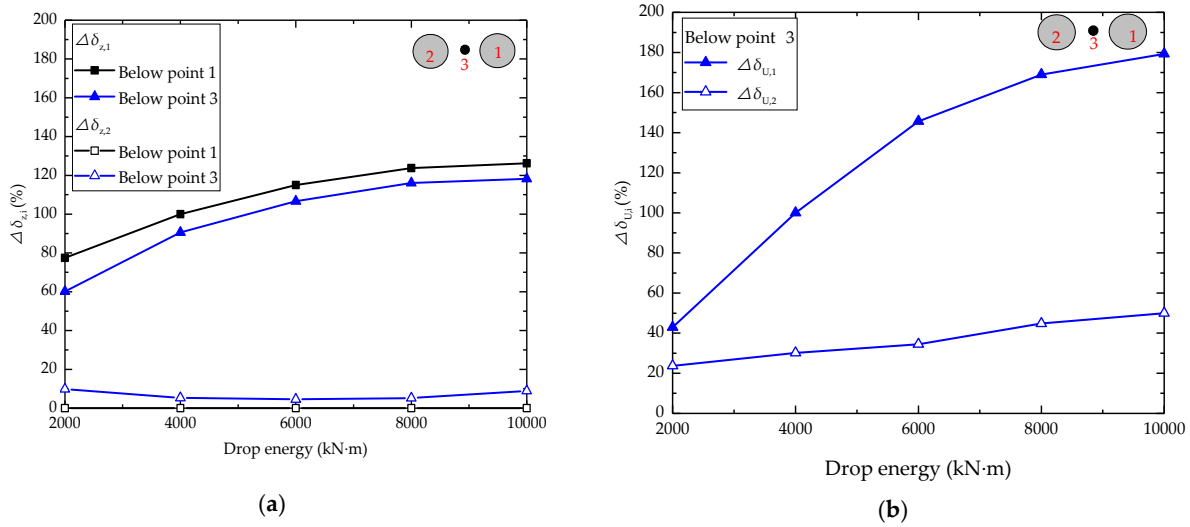

(**a**) (**b**)

Figure 12. Normalized indicators versus drop energy: (**a**) $\Delta\delta_{z,i}$; (**b**) $\Delta\delta_{U,i}$.

3.4. Effect of Tamping Distance

The numerical simulation of DC is performed with tamper radius R = 1.2 m, drop energy MH = 4000 kN·m, tamping distances (S) ranging from 3.6 to 10.8 m, and blows of 10 at each impact point to investigate the influence of tamping distance on multipoint tamping.

Figure 13 shows the zone of I_r = 7.7% for different tamping distances. The increasing tamping distance leads to the decrease in the overlap of the contour line, the influence depth, and soil improvement between impact points, whereas the influence width has a positive effect on tamping distance. Figure 14 shows the value of I_r reduces with the increasing tamping distance. It is observed that impact at points 1 and 2 slightly influences the soil improvement between impact points when the tamping distance exceeds 4.5 D, and the soil improvement will be relatively poor.

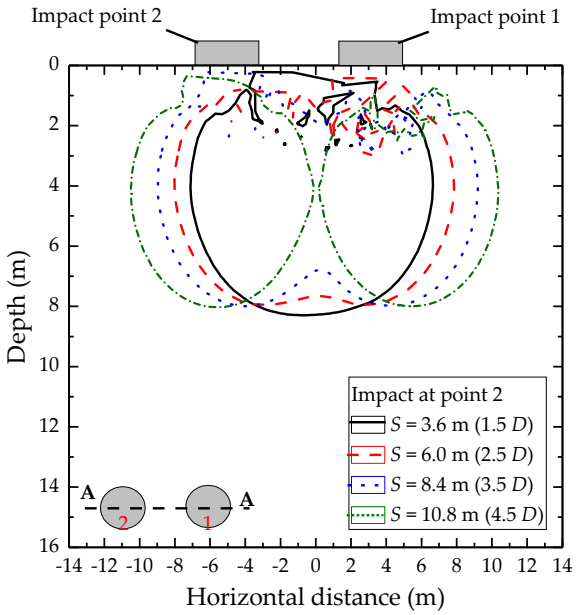

Figure 13. The zone of I_r = 7.7% for tamping distance.

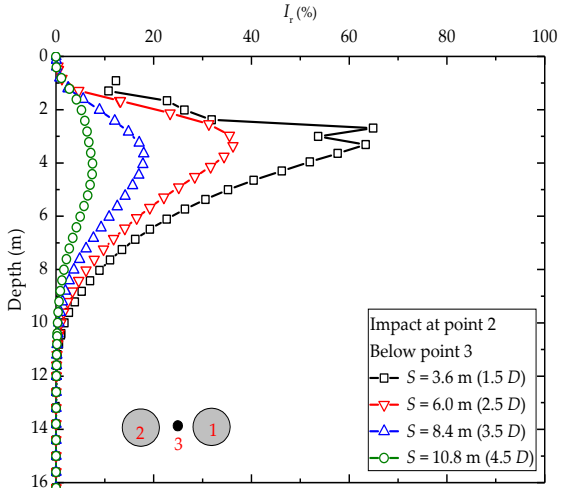

Figure 14. I_r of soil versus depth for tamping distance.

Figures 15 *s*hows that with the increase in *S*/*D*, both $\Delta\delta_{z,1}$ and $\Delta\delta_{U,1}$ during impact at point 1 decrease continually and reach the value of 0% and 25% when *S*/*D* =4.5, indicating that the increase in *S*/*D* will produce weaker compaction effect between impact points. It needs to be pointed out that during impact at point 2 a relatively low value of $\Delta\delta_{z,2}$ approximately 10% is observed and$\Delta\delta_{U,2}$ increases from 3% when *S*/*D* = 1.5 to about 30% when *S*/*D* = 2.5 and then decreases from 30% when *S*/*D* = 2.5 to about 7% when *S*/*D* = 4.0. It means $\Delta\delta_{U,2}$increases with the *S*/*D* first and then decreases during impact at point 2. The results show that the tamping distance about 2.5 times of tamper diameter (2.5 *D*) is the most efficient in soil improvement between impact points during impact at point 2. Figure 15b also shows that the first impact points play a major role in the compaction effect between impact points.

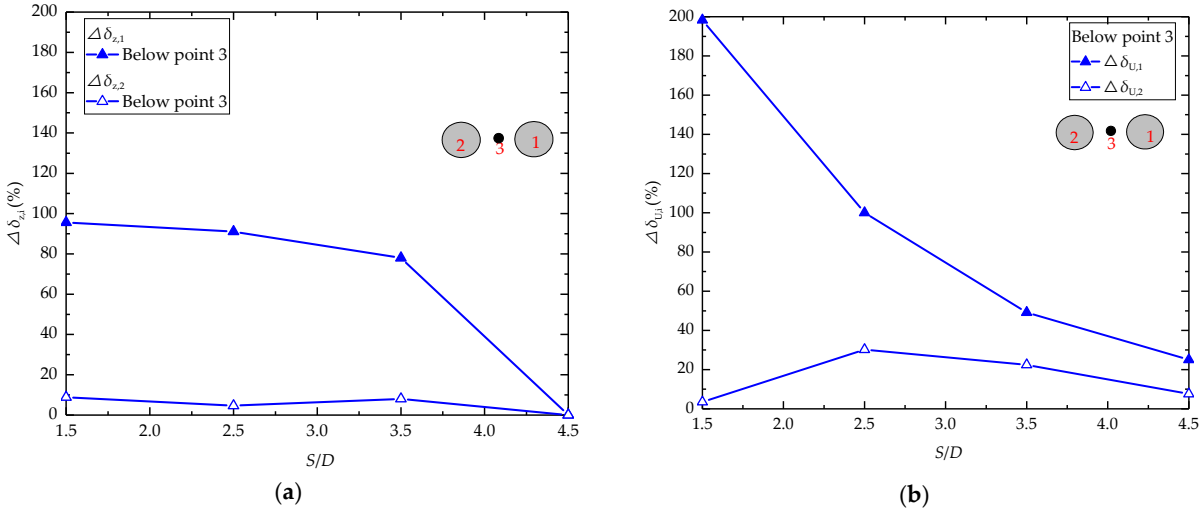

Figure 15. Normalized indicators versus *S*/*D*: (**a**) $\Delta\delta_{z,i}$; (**b**) $\Delta\delta_{U,i}$.

3.5. Effect of Tamper Radius

The numerical simulation of DC is performed with a tamping distance *S* = 6.0 m, drop energy *MH* = 4000 kN·m, tamper radius (*R*) ranging from 0.6 to 3.0 m, and the blows of 10 at each impact point to investigate the influence of the tamper radius on the soil improvement.

As is expected in Figure 16a, for the case of the single-point tamping, a larger radius leads to a smaller improvement depth due mainly to the lower impact stress. Besides, a wider improvement zone can be achieved by using a tamper with a larger radius. It can

also be seen in Figure 16b, for the case of the multipoint tamping, that an increase of the tamper radius leads to a wider improvement area, while a slightly less improvement depth between impact points was observed.

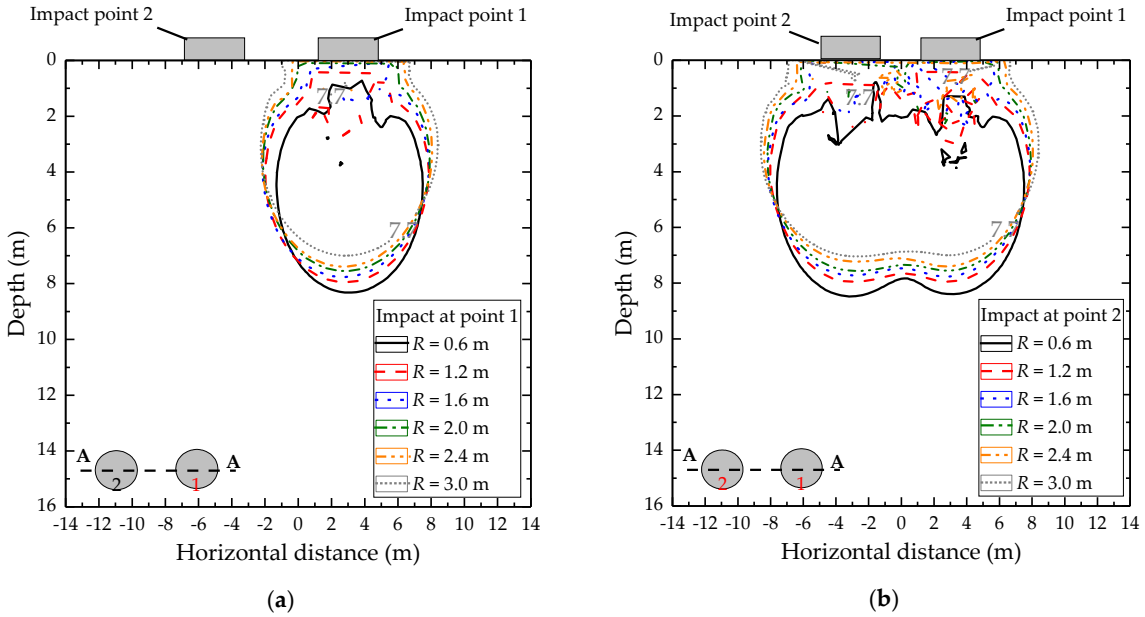

Figure 16. The zone of I_r = 7.7% for tamper radius: (**a**) impact at point 1; (**b**) impact at point 2.

Closer inspection of Figure 17 indicates that the smaller the tamper radius, the better the improvement effect, and the more pronounced the effect of the tamper on the location of point 1. This is consistent with the results obtained by Yong [32]. However, a less improvement effect was observed between the impact points. The results indicated that DC can be effectively employed to improve local reinforcement effects as the dimension of the tamper reduces. Besides, I_r below point 3 is little affected by the tamper radius. This is consistent with the observation of $\delta_{z,2}$, and $\delta_{U,2}$ in Figure 22.

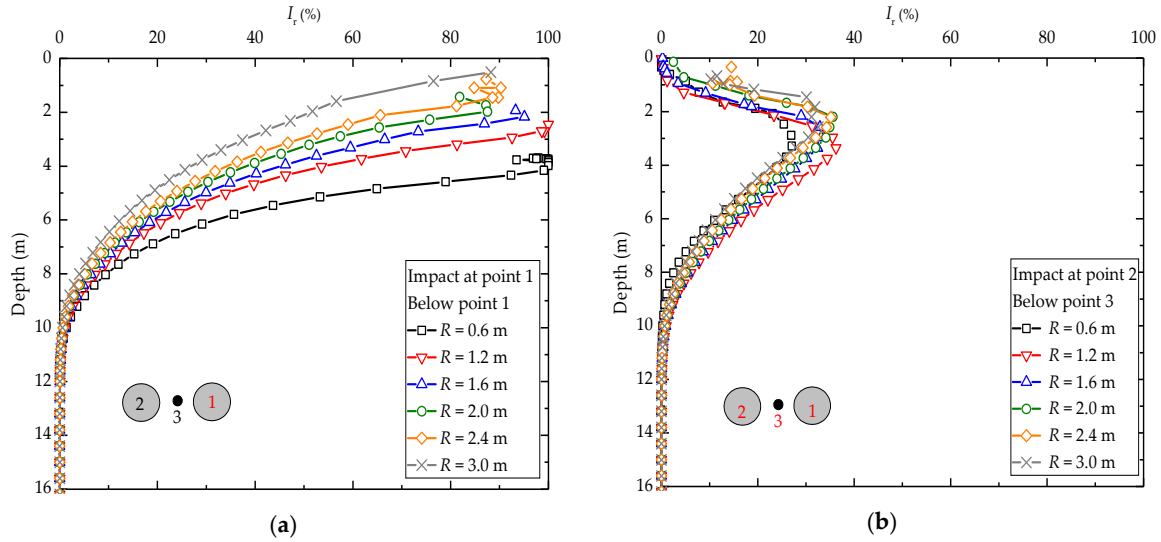

Figure 17. I_r of soil versus depth for tamper radius: (**a**) below point 1; (**b**) below point 3.

Figure 18a shows that $\Delta\delta_{z,i}$ (i = 1,2) below points 1 and 3 decreases slightly with tamper radius, indicating that the soil improvement affected by the tamper radius is so little that it can be negligible. Figure 18b shows that $\Delta\delta_{U,1}$ increases from 70% when R = 0.5 m to about 106% when R = 1.6 m and then decreases from 106% when R = 1.6 m to about 94%

when R = 3.0 m during impact at point 1, while $\Delta\delta_{U,2}$ changes little with the increase in tamper radius during impact at point 2. This suggests that for a given weight of tamper, there is an optimum tamper radius to optimize soil improvement between impact points during impact at point 1, which is consistent with Lee and Gu's findings [10]. Figure 18b also shows that there exists the attenuation of the compaction effect between impact at points 1 and 2.

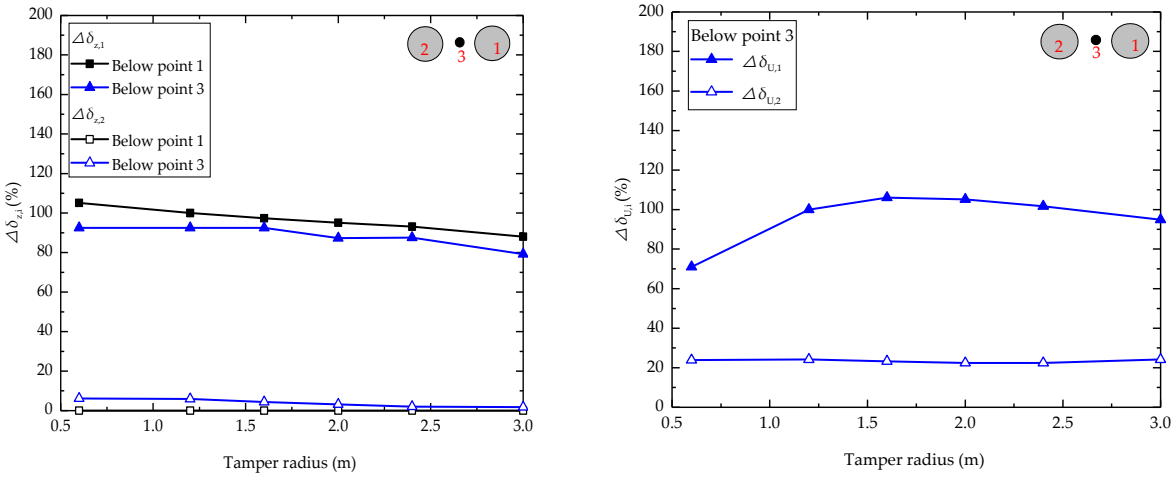

(**a**) (**b**)

Figure 18. Normalized indicators versus tamper radius: (**a**) $\Delta\delta_{z,i}$; (**b**) $\Delta\delta_{U,i}$.

3.6. Effect of the Different Combinations of Tamper Mass and Drop Height

The numerical simulations are performed to investigate the effect of the combinations of tamper mass and drop height on the improvement effect, taking the combinations of 4000 kN·m with different tamper mass and drop height as an example.

Figures 19 and 20 show that a wider extent of the improvement is observed by using a low drop of a heavy tamper than that of a high drop of a light tamper. This is consistent with the observations in the literature [9,30] that a low drop of a heavy tamper is more beneficial to the expansion of the improvement range. The extent of improvement induced by the tamper with a weight of 40 tons and tamper with a weight of 50 tons appear to be identical, indicating that further increase in the tamper mass has no obvious effect on the relative degree of improvement. Moreover, the drop energy remains constant as 4000 kN·m, but the drop momentum is varied with a different combination of tamper mass and drop height, as shown in Table 5. Oshima and Takada [13] indicate that drop momentum can be used to estimate the crater depth and improvement area when the drop energy is constant. It can be defined as $M_v = MV = M\sqrt{2gH}$, where M is the tamper mass, H is the drop height, V is the impact speed. Thus, drop momentum can be used to describe the physical quantity of the impact load and evaluate the improvement effect under the same drop energy with different combinations of the tamper mass and drop height.

Table 5. Parameters of the tamper with different drop momentum.

***M* (tons)**	15	20	30	40	50
***H* (m)**	26.6	20	13.4	10	8
Drop momentum (tons m/s)	273.3	400	491.1	565.6	632.4

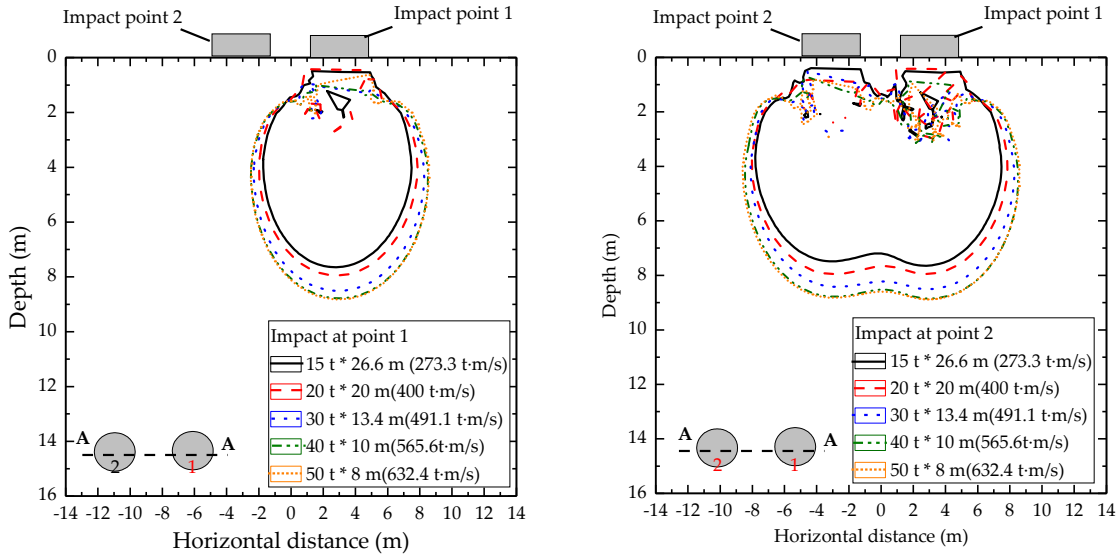

Figure 19. The zone of $I_r = 7.7\%$ for different combinations of the tamper mass and the drop height: (**a**) impact at point 1; (**b**) impact at point 2.

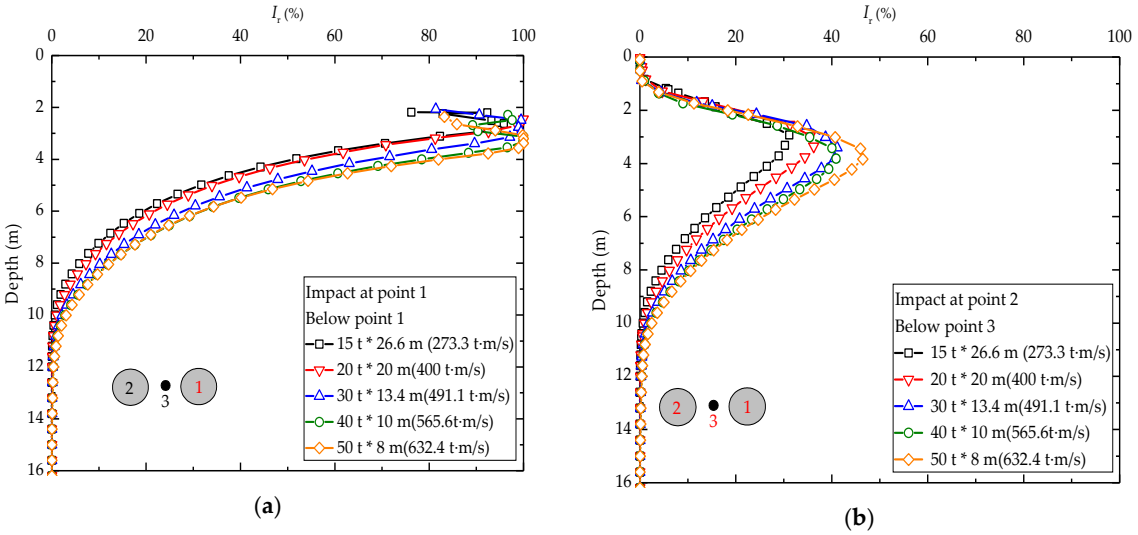

Figure 20. I_r of soil versus depth for different combinations of the tamper mass and the drop height: (**a**) below point 1; (**b**) below point 3.

As shown in Figure 21, both $\Delta\delta_{z,1}$ and $\Delta\delta_{U,1}$ increase gradually with the drop momentum, which is consistent with the results in Figures 19 and 20. It means that under the same drop energy a lower drop of a heavy tamper (i.e., the combination of the tamper with a weight of 50 tons and the drop height of 8.0 m) has a deeper improvement depth and better improvement effect between impact points than a high drop of a light tamper (i.e., the combination of the tamper with a weight of 15 tons and the drop height of 26.6 m). Figure 21b shows that the soil improvement between the impact points may experience attenuation when impact at point 2.

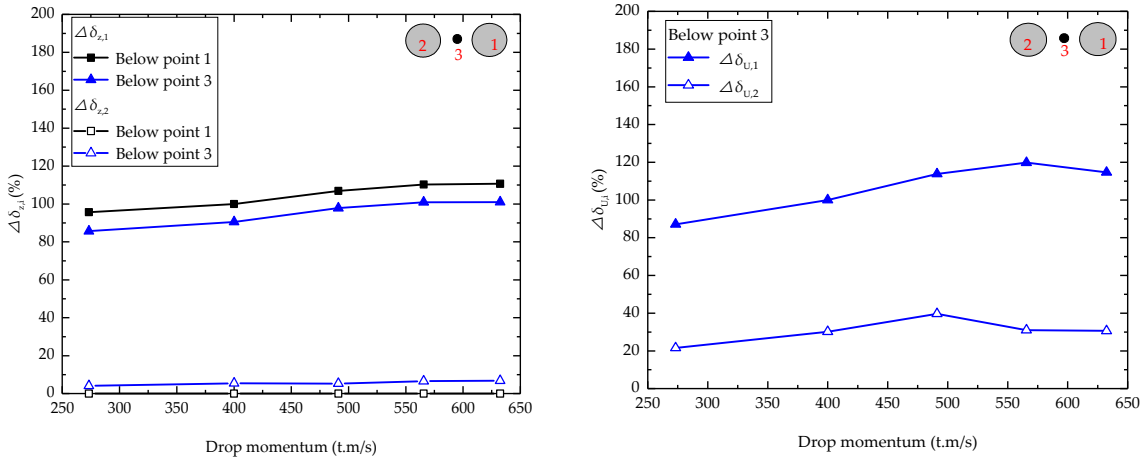

Figure 21. Normalized indicators versus different combinations of the tamper mass and the drop height: (**a**) $\Delta\delta_{z,i}$; (**b**) $\Delta\delta_{U,i}$.

3.7. Sensitivity Analysis of Multipoint Tamping

The *x*-axis label "The multiple change of parameters" in Figure 22 means the corresponding normalized parameter indicators such as drop number, tamper radius, drop energy and tamping distance are given normalized treatment by the case of the numerical model with $S = 6.0$ m, $MH = 4000$ kN·m, $R = 1.2$ m and $N = 10$ after impact at point 1. Figure 22 shows the sensitivity analysis of the influencing factors mentioned above in the case of multipoint tamping. It can be found that the effects of parameters are different: the increase in drop energy and drop momentum play the most important roles in the expansion of the improvement area, improvement depth, and the soil improvement between impact points; the increase in S is more beneficial to the improvement area but less to the improvement depth and soil improvement between impact points; the increase in N has a certain influence on the improvement of both shallow and deep soils; R has little effect on the improvement of both shallow and deep soils.

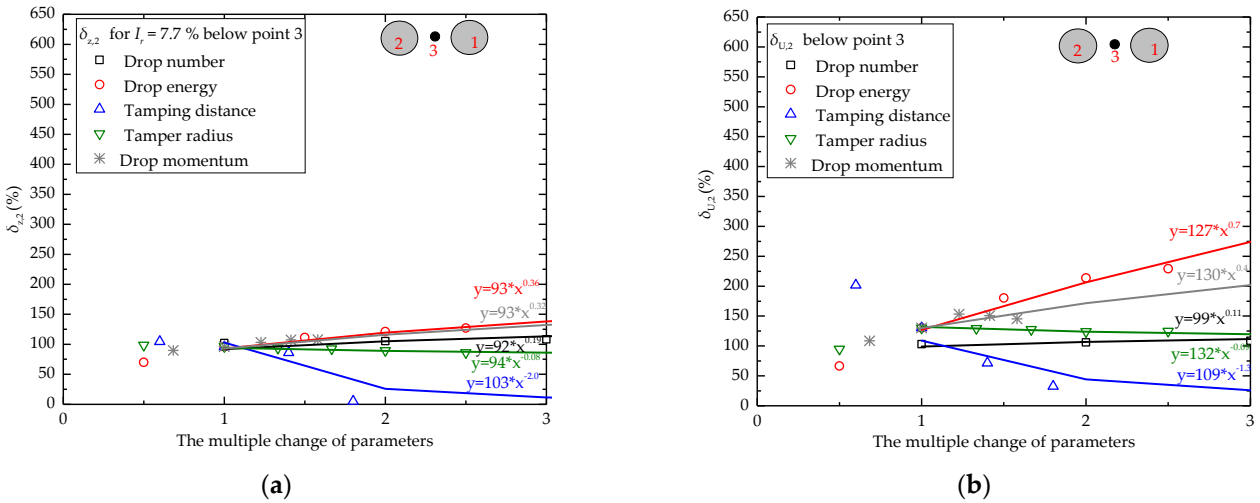

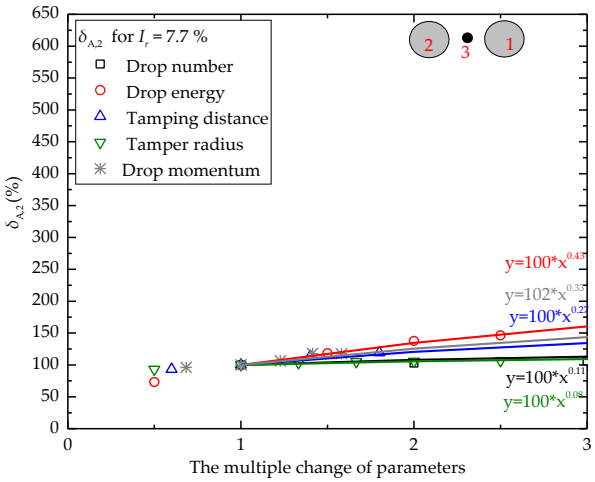

(**c**)

Figure 22. The sensitivity analysis for the multipoint tamping: (**a**) $\delta_{z,2}$; (**b**) $\delta_{U,2}$; (**c**) $\delta_{A,2}$.

4. Proposition and Application of Prediction Formula

4.1. Degree of Soil Improvement with Depth

Chow et al. [19] concluded that the better and the least soil improvement zones are below the impact point and at the middle of impact points, respectively. Thus, these two points (points 1 and 3 as shown in Figure 23) are used as the ideal quality control points for DC treatment in this section.

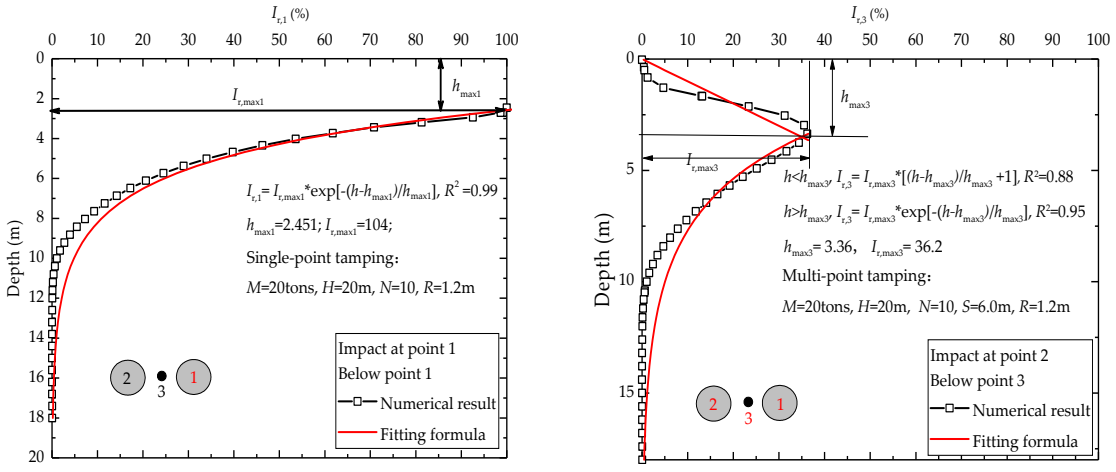

(**a**) (**b**)

Figure 23. Schematic diagram of DC: (a) below point 1; (b) below point 3.

For point 1 by single-point tamping, the variation of the value of $I_{r,1}$ with the depth can be roughly represented by an exponential formula, and the fitting formula is:

$$I_{r,1} = I_{r,\max 1} \exp\left(-\frac{h - h_{\max 1}}{h_{\max 1}}\right) \quad (8)$$

For point 3 by multipoint tamping, the relationship between the depth and the value of $I_{r,3}$ can be fitted using the following piecewise function, and the formulas are:

$$I_{r,3}=\begin{cases} I_{r,\max 3}\left[\left(\dfrac{h-h_{\max 3}}{h_{\max 3}}\right)+1\right], \; if\, h \le h_{max3} \\ I_{r,\max 3}\exp\left(-\dfrac{h-h_{\max 3}}{h_{\max 3}}\right), \; if\, h > h_{max3} \end{cases} \quad (9)$$

where $I_{r,max1}$, $I_{r,max3}$, h_{max1}, and h_{max3} are the maximum value of I_r, and the corresponding depth in the cases of single-point or multipoint tamping, as shown in Figure 23.

Figures 24 and 25 show that the correlation coefficient *R*-value of the normalized $I_{r,1}/I_{r,max1}$ and $I_{r,3}/I_{r,max3}$ between the numerical results and those derived by Equations (8) and (9) are relatively higher than 90%. However, it appears to be over-estimated for different construction parameters in the zone ranging from 2 to 3 of normalized depth. This may be attributed to the exponential function that is used in the analysis. The differences bring relatively lesser impact on this estimation method, which has been proved by Figures 27 and 28. Thus, we can assume that the effect of the influence factor on the zone of improvement can be approximatively "eliminated" by using Equations (8) and (9).

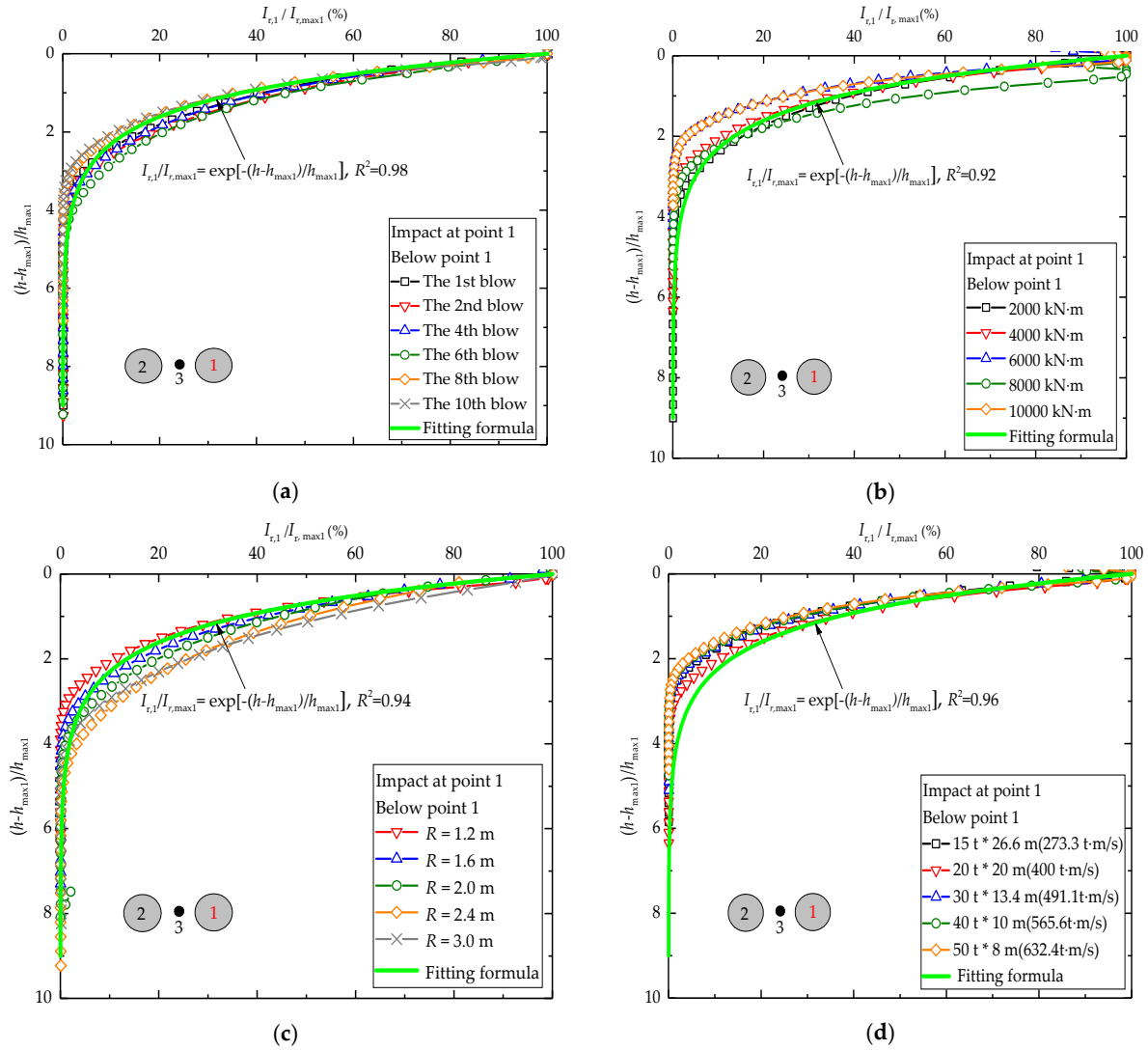

Figure 24. Normalized $I_{r,1}$ /$I_{r,\max 1}$ (%) and $(h\text{-}h_{max1})/h_{max1}$ for construction parameter: (**a**) drop number; (**b**) drop energy; (**c**) tamper radius; (**d**) drop momentum.

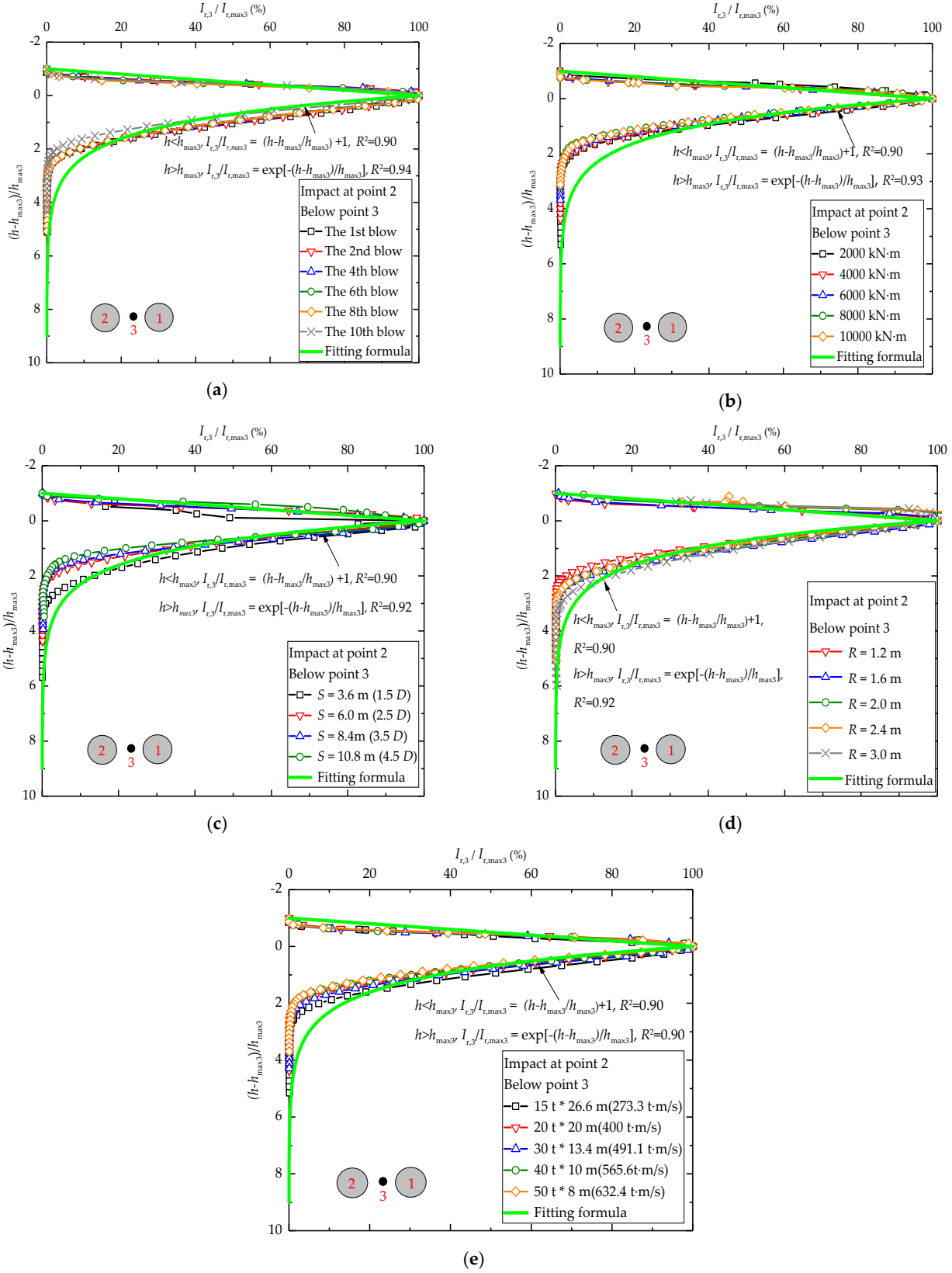

Figure 25. Normalized $I_{r,3}$ /$I_{r,\max 3}$ (%) and $(h\text{-}h_{max3})/h_{max3}$ for construction parameter: (a) drop number; (b) drop energy; (c) tamping distance; (d) tamper radius; (e) drop momentum.

According to Zhang et al. [30], the coefficient $I_{r,max1}$, h_{max1}, $I_{r,max3}$, and h_{max3} can be determined by using the following expressions:

$$I_{\mathrm{r,max1}} = k_1 N^{k_2} \left(MH\right)^{k_3} R^{k_4} \tag{10}$$

$$h_{\mathrm{max1}} = l_1 N^{l_2} \left(MH\right)^{l_3} R^{l_4} \tag{11}$$

$$I_{\mathrm{r,max3}} = e_1 N^{e_2} \left(MH\right)^{e_3} \left(\frac{S}{D}\right)^{e_4} \tag{12}$$

$$h_{\mathrm{max3}} = f_1 N^{f_2} \left(MH\right)^{f_3} \left(\frac{S}{D}\right)^{f_4} \tag{13}$$

where k_1, k_2, k_3, k_4; l_1, l_2, l_3, l_4; e_1, e_2, e_3, e_4 and f_1, f_2, f_3, f_4 are the fitting coefficients that need to be determined.

A total number of 17 numerical simulations (See Table 3) with varied drop energy (MH), drop number (N), tamping distance (S), different combinations of 4000 kN·m and tamper radius (R) are performed by using a statistical analysis software SPSS (Statistical Package for the Social Sciences) program to determine the relevant parameter. Table 6 shows the curve-fitting coefficients and R-square of Equations (10)–(13).

Table 6. Curve-fitting coefficients of Equations (10)–(13).

Equation	Fitting Coefficients				*R*-Square
Equation (10)	k_1	k_2	k_3	k_4	0.90
	0.32	0.34	0.072	−0.44	
Equation (11)	l_1	l_2	l_3	l_4	0.93
	0.21	0.22	0.35	−0.50	
Equation (12)	e_1	e_2	e_3	e_4	0.94
	0.9	0.23	0.54	0.20	
Equation (13)	f_1	f_2	f_3	f_4	0.91
	0.26	0.26	0.28	0.29	

The instruction of the estimation method for the improvement effect of the sandy soil is shown in Figure 26. The flow chart provides step-by-step instructions on how civil engineers can use the proposed formula to estimate soil improvement after DC.

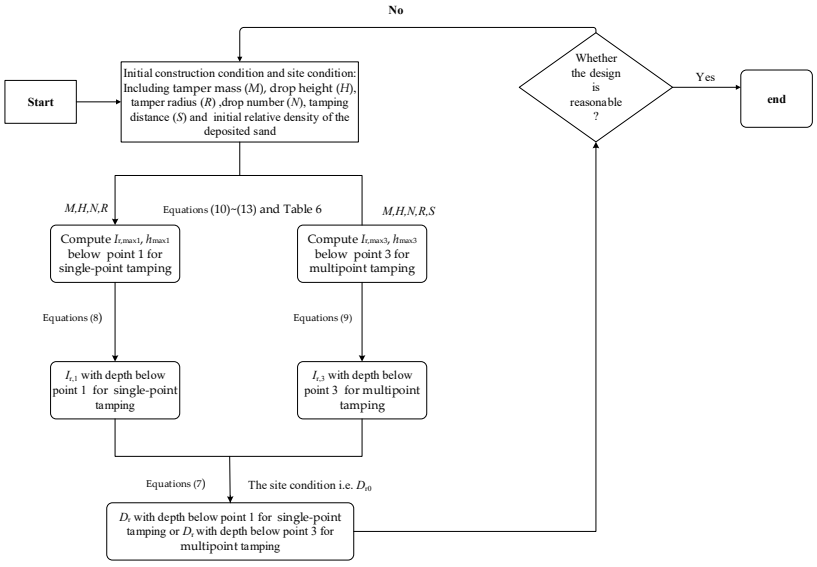

Figure 26. Flow chart of the estimation method for dynamic compaction (DC) of granular soils.

4.2. Verification of the Prediction Formula

In this section, a preliminary assessment of the reliability of the proposed formula to predict the relative density after DC is carried out for the Changi Airport site [6,22] and the Kampung Pakar site [10,19,22]. Table 7 shows the details of DC in the two field cases. It should be noted that the prediction formula is based on two impact points, whereas there exists the square of tamping in the field cases. Thus, the diagonal tamping distance of field cases is used to replace the tamping distance of Equations (12) and (13) in the verification of the prediction formula [22].

Table 7. Details of DC at two field cases.

Site Location	*M* (tons)	*H* (m)	*D* (m)	*S* (m)	*N*	Type of Soil
Changi Airport	23	25	2.65	6	10	Highly permeable sandy soil
Kampung Pakar	15	20	2.06	6	10	

4.2.1. Changi Airport Site, Singapore

The Changi East Reclamation Project is in Singapore. A reclaimed sandfill with an average of 10–12 m thickness is treated by DC to meet the construction requirement. The water table is about 1 m below the fill [19,22]. According to Dou et al. [22], the initial relative density D_{r0} is 44%.

Figure 27 shows the curve obtained by the proposed fitting formula and those estimated from measured data after DC at the Changi Airport site. It can be found that the variation tendency in the relative density with depth in the improvement zone is similar to that estimated from the measured data.

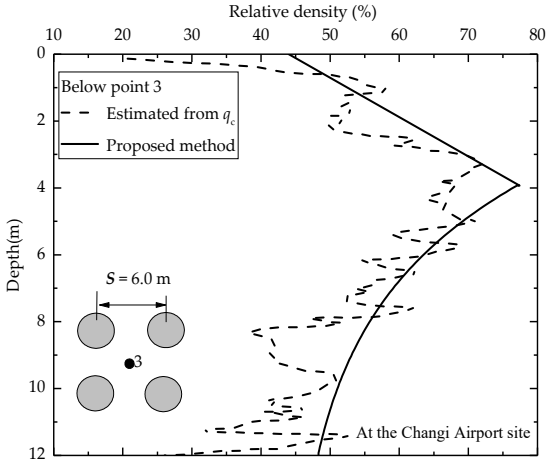

Figure 27. Measured relative density and estimated relative density in the center of the square of tamping.

4.2.2. Kampung Pakar Site, Malaysia

The Kampung Pakar site is situated in Sungei Besi, Malaysia. The soil deposit is constituted by 14 m of loose sand with a layer of silty clay at 10-12 m. The water table is about 3 m below the surface. The initial relative density of 46% is based on Lee and Gu [10] and Dou et al. [22].

As shown in Figure 28, there is a reasonable agreement between the proposed fitting formula and the relative density estimated from q_c. However, the relative density appeared to be over-estimated in the zone near the surface, between 0 and 3 m depth (in Figure 28a). This may be attributed to the fact that the soil near the surface is a dilation zone with little soil improvement in the field test, while the cap surface expands

continuously with the increase in the drop number. Thus there exists a calculation error near the surface, between 0 and 3 m depth.

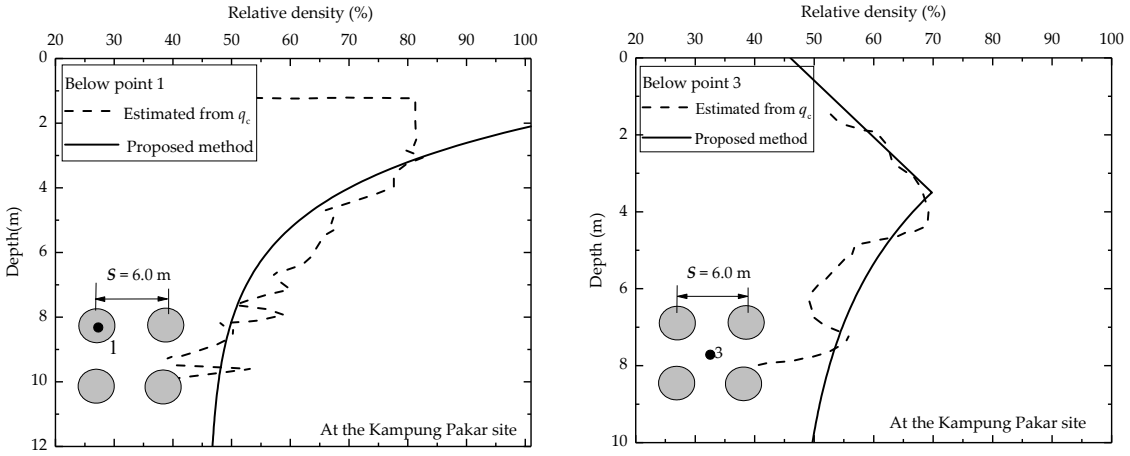

(**a**) (**b**)

Figure 28. Measured relative density and estimated relative density: (**a**) below point 1; (**b**) in the center of the square of tamping.

5. Discussion and Conclusions

In this paper, the numerical investigation is carried out using 3D FEM. An improved soil cap model realizes the variation of elastic parameters during the DC process. The feasibility of the models is supported by comparison with centrifuge model results. Based on the numerical results, the following conclusions can be made:

1. As for single-point and multipoint tamping, the drop energy and drop momentum exert significant effects on the effective improvement depth and soil improvement between the impact points, whereas the influence of the drop number and the tamper radius is relatively smaller.
2. There exists saturated drop energy beyond which further energy application has little effect on soil improvement. Under the same condition of drop energy, a low drop of a heavy tamper can generate a larger improvement area, a deeper improvement depth, and is more conducive to the soil improvement between impact points.
3. The increase in tamping distance is more beneficial to the improvement area but less to the improvement depth and soil improvement between impact points. Beyond a certain tamping distance, the impact at points 1 and 2 slightly influences the soil improvement between impact points, and soil improvement between impact points will be relatively poor.
4. The soil compacted between impact points by the previous impact point will be improved to a lesser extent with impact at subsequent impact points.
5. The most significant finding from this paper is the proposed method of evaluating the sandy soil improvement effect of DC according to specified engineering requirements. It not only predicts the degree of final improvement with depth both below impact point and between impact points but also provides the optimal technological parameters for DC construction.

It is important to note, however, that DC partly relies on soil liquefying locally and densifying through the dissipation of the excess pore pressures. These features of the response cannot be replicated with the adopted constitutive model. Thus, the proposed method is applied strictly only to moist and dry granular soils. Developing a more practical model deserves further investigation in the future.

Author Contributions: Methodology, writing—original draft, C.Z.; software, validation, C.Z., H.L., and C.Y.; conceptualization, formal analysis, writing—review and editing, C.Z.; supervision, K.Y, and Z.Y.; project administration, H.Q., K.W, and P.J. All authors have read and agreed to the published version of the manuscript.

Funding: This research received no external funding

Institutional Review Board Statement: Not applicable.

Informed Consent Statement: Not applicable.

Data Availability Statement: Data sharing not applicable.

Conflicts of Interest: The authors declare no conflict of interest.

References

1. Mayne, P.W.; Jones, J.S., Jr.; Dumas, J.C. Ground response to dynamic compaction. *J. Geotech. Eng.* **1984**, *110*, 757–774.
2. Shenthan, T.; Nashed, R.; Thevanayagam, S. Liquefaction mitigation in silty soils using composite stone columns and dynamic compaction. *Earthq. Eng. Eng. Vib.* **2004**, *3*, 39–50.
3. Menard, L.; Broise, Y. Theoretical and practical aspect of dynamic consolidation. *Geotechnique* **1975**, *25*, 3–18.
4. Van Impe, W.F.; Bouazza, A. Densification of domestic waste fills by dynamic compaction. *Can. Geotech. J.* **1997**, *33*, 879–887.
5. Feng, S.J.; Du, F.L.; Shi, Z.M.; Shui, W.H.; Tan, K. Field study on the reinforcement of collapsible loess using dynamic compaction. *Eng. Geol.* **2015**, *185*, 105–115.
6. Bo, M.W.; Na, Y.M.; Arulrajah, A.; Chang, M.F. Densification of granular soil by dynamic compaction. *Proc. Inst. Civ. Eng. Ground Improv.* **2009**, *162*, 121–132.
7. Lukas, R.G. *Dynamic Compaction of Highway Construction, Design and Construction Guidelines*; Report No. FHWA/RD-86/133; Fedral Highway Administration: Washington, DC, USA, 1986.
8. Poran, C.J.; Rodriguez, J.A. Design of dynamic compaction. *Can. Geotech. J.* **1992**, *29*, 796–802.
9. Gu, Q.; Lee, F.H. Ground response to dynamic compaction of dry sand. *Geotechnique* **2002**, *52*, 481–493.
10. Lee, F.H.; Gu, Q. Method for estimating dynamic compaction effect on sand. *J. Geotech. Geoenviron. Eng.* **2004**, *130*, 139–152.
11. Zhou, C.; Jiang, H.; Yao, Z.; Li, H.; Yang, C.; Chen, L.; Geng, X. Evaluation of dynamic compaction to improve saturated foundation based on the fluid-solid coupled method with soil cap model. *Comput. Geotech.* **2020**, *125*, 103686.
12. Wang, W.; Chen, J.J.; Wang, J.H. Estimation method for ground deformation of granular soils caused by dynamic compaction. *Soil Dyn. Earthq. Eng.* **2017**, *92*, 266–278.
13. Oshima, A.; Takada, N.; Tanaka, Y. Relation between compacted area and ram momentum by heaving tamping. *Doboku Gakkai Ronbunshu* **1996**, *554*, 185–196.
14. Oshima. A.; Takada, N. Evaluation of compacted area of heavy tamping by cone point resistance. In Proceedings of the International Conference of Centrifuge, Tokyo, Japan, 1998-09-23; pp. 813–818.
15. Lukas, R.G. *Geotechnical Engineering Circular, Dynamic Compaction*; Report No. FHWA/SA -95/037; Fedral Highway Administration: Washington, DC, USA, 1995.
16. Feng, S.J.; Tan, K.; Shui, W.H. Dynamic compaction of ultra-high energy in combination with ground replacement in coastal reclamation areas. *Mar. Geores. Geotechnol.* **2015**, *33*, 109–121.
17. Feng, S.J.; Shui, W.H.; Gao, L.Y.; Tan, K. Field studies of the effectiveness of dynamic compaction in coastal reclamation areas. *Bull. Eng. Geol. Environ.* **2010**, *69*, 129–136.
18. Feng, S.J.; Shui, W.H.; Tan, K. Field evaluation of dynamic compaction on granular deposits. *J. Perform. Constr. Facil.* **2011**, *25*, 241–249.
19. Chow, Y.K.; Yong, D.M.; Yong, K.Y.; Lee, S.L. Dynamic compaction of loose granular soils: Effect of print spacing. *J. Geotech. Eng.* **1994**, *120*, 1115–1133.
20. Jahangiri, G.; Pak, A.; Ghassemi, A. Numerical modelling of dynamic compaction in dry sandy soils for determination of effective print spacing. *J. Struct. Eng. Geotech.* **2011**, *1*, 27–35.
21. Wang, W.; Dou, J.; Chen, J.; Wang, J. Numerical analysis of the soil compaction degree under multi-location tamping. *J. Shanghai Jiaotong Univ. (Sci.)* **2017**, *22*, 417–433.
22. Dou, J.; Chen, J.; Wang, W. Method for Estimating the Degree of Improvement in Soil between Adjacent Tamping Locations under Dynamic Compaction. *Int. J. Geomech.* **2019**, *19*, 04019134.
23. Zhang, F.; Wang, B.; Liu, H.; Zhu, Z. Application of dynamic compaction to foundation improvement of a flood-prevention dam in Yibin. *Rock. Soil. Mech.* **2004**, *25*, 490–494. (In Chinese)
24. Wang, B.; Zhang, F.; Zhu, Z. Effectiveness detection of dynamic compaction on silt foundations of a flood-prevention dyke at Yibin. *Rock. Soil. Mech.* **2004**, *25*, 1159–1162. (In Chinese)
25. Lv, X.; Gong, X.; Li, J. Research on parameters of construction with dynamic compaction method. *Rock. Soil. Mech.* **2006**, *9*, 1628–1632. (In Chinese)
26. Li, B.H.; An, M. Discussion on Compaction Spacing and Arrangement Form of Dynamic Compaction Method. *Constr. Technol.* **2007**, *9*, 55–57. (In Chinese)

27. Helwany, S. *Applied Soil Mechanics with ABAQUS Applications*; John Wiley and Sons: Hoboken, NJ, USA, 2007.
28. Ghassemi, A.; Pak, A.; Shahir, H. Validity of Menard relation in dynamic compaction operations. *Proc. Inst. Civ. Eng. Ground Improv.* **2009**, *162*, 37–45.
29. Poran, C.J.; Rodriguez, J.A. Finite element analysis of impact behavior of sand. *Soils Found.* **1992**, *32*, 68–80.
30. Zhang, R.; Sun, Y.; Song, E. Simulation of dynamic compaction and analysis of its efficiency with the material point method. *Comput. Geotech.* **2019**, *116*, 103218.
31. Jia, M.; Zhao, Y.; Zhou, X. Field Studies of Dynamic Compaction on Marine Deposits. Mar. Geores. Geotechnol. 2016, 34, 313–320.
32. Yong, D.M. Ground Improvement by Dynamic Compaction. Ph.D. Thesis, National University of Singapore, Singapore, 1993; pp. 88–91.